Molecular Vision 2018; 24:115-126 <http://www.molvis.org/molvis/v24/115>
Received 7 June 2017 | Accepted 1 February 2018 | Published 3 February 2018

The genetic dissection of *Myo7a* gene expression in the retinas of BXD mice

Ye Lu,[1] Diana Zhou,[2] Rebecca King,[3] Shuang Zhu,[4] Claire L. Simpson,[2] Byron C. Jones,[2] Wenbo Zhang,[4] Eldon E. Geisert,[3] Lu Lu[2]

(The first two authors contributed equally to this work.)

[1]Department of Ophthalmology, The First Affiliated Hospital, Zhejiang University College of Medicine, Hangzhou, China; [2]Department of Genetics, Genomics and Informatics, University of Tennessee Health Science Center, Memphis, TN; [3]Department of Ophthalmology and Emory Eye Center, Emory University, Atlanta, GA; [4]Department of Ophthalmology & Visual Sciences, University of Texas Medical Branch, Galveston, TX

Purpose: Usher syndrome (US) is characterized by a loss of vision due to retinitis pigmentosa (RP) and deafness. US has three clinical subtypes, but even within each subtype, the severity varies. Myosin VIIA, coded by *Myo7a*, has been identified as one of the causal genes of US. This study aims to identify pathways and other genes through which *Myo7a* interacts to affect the presentation of US symptoms.
Methods: In this study, we used the retinal tissue of BXD recombinant inbred (RI) mice to examine the expression of *Myo7a* and perform genetic mapping. Expression quantitative trait locus (eQTL), single nucleotide polymorphism (SNP), and gene correlation analysis were performed using GeneNetwork. Gene set enrichment analysis was performed using WebGestalt, and gene network construction was performed using the Gene Cohesion Analysis Tool.
Results: We found *Myo7a* to be *cis*-regulated, with varied levels of expression across BXD strains. Here, we propose a genetic network with 40 genes whose expression is highly correlated with *Myo7a*. Among these genes, six have been linked to retinal diseases, three to deafness, and five share a transcription factor with *Myo7a*. Gene ontology and pathway analysis revealed a strong connection among ion channel activity, *Myo7a*, and US.
Conclusions: Although *Myo7a* is a causal gene of US type I, this gene works with many other genes and pathways to affect the severity of US. Many of the genes found in the genetic network, pathways, and gene ontology categories of *Myo7a* are related to either deafness or blindness. Further investigation is needed to examine the specific relationships between these genes, which may assist in the treatment of US.

The human unconventional myosin VIIa (*MYO7A*, Gene ID 4647, OMIM 276903) gene is located on chromosome 11q13.5 and encodes the protein myosin VIIA, which is part of the unconventional myosins group. These proteins interact with actin and facilitate molecular transport within cells. Myosin VIIA is primarily expressed in the cochlear and vestibular neuroepithelia of the inner ear and in the retinal pigment epithelium (RPE) and photoreceptors. In the retina, myosin VIIA supports and maintains nourishment of the RPE. Myosin VIIA normally carries small sacs of pigment called melanosomes within the RPE, which are necessary for normal vision. Myosin VIIA is also found in other parts of the retina, where this protein most likely carries proteins and molecules important to vision, and is involved in the phagocytosis of disk membranes involved in normal sight [1]. Mutations in *Myo7a* have been known to cause Usher syndrome (US), a disorder affecting the ear and the retina.

US is an autosomal recessive genetic disorder that causes loss in vision, hearing, and vestibular function. Patients with US often develop inner ear defects and degeneration of retinal cells (retinitis pigmentosa, or RP). Combined, these symptoms lead to complete or partial loss of sight or hearing or both. The expression of US is highly variable in different individuals. The clinical and genetic heterogeneity of US shows that this trait is complex, with primary causal genes interacting with other coexpression genes to produce the clinical presentation. Globally, mutations in *MYO7A* are the most common cause of US type 1, accounting for anywhere between 29% and 75% of cases [2-8]. These mutations may also account for some cases of type 2 [7,9] and the atypical type 3 [10]. Even within type 1, there are wide phenotypic variations, and there has been much hypothesizing on the genotype–phenotype relationships between the various mutations in *MYO7A* and the diversity of clinical presentations. To date, our understanding of why such wide heterogeneity exists in US cases remains poor, although there is some evidence that null mutations may

Correspondence to: Lu Lu, 71 S. Manassas St, Department of Genetics, Genomics and Informatics, University of Tennessee Health Science Center, Memphis, TN, 38163; Phone: (901) 448-7557; FAX: (901) 448-3500; email: lulu@uthsc.edu

result in milder phenotypes [11]. Mutations in *MYO7A* almost always present as autosomal recessive, with either true homozygotes or compound heterozygotes being affected with the disease. However, there are specific instances of autosomal dominant inheritance where interaction with the wild-type protein produces a dominant-negative effect. In addition, there is now evidence that other genetic factors may affect the penetrance of mutations in *MYO7A* [12,13], and this may account for some of the observed variability in the phenotype.

Recombinant inbred (RI) mice are a powerful tool for systems genetics analysis. The current largest panel of these strains—the BXD family—consists of more than 100 strains derived from a cross between the C57BL/6J strain (B6), which has no aberrant ocular phenotype, and the DBA/2J strain (D2), which harbors mutations in several genes that result in some aberrant ocular phenotypes. For example, after 6 months of age, most D2 mice develop iris depigmentation and increased intraocular pressure (IOP) followed by damage to the optic nerve [14]. Mutations in two genes are already known to contribute to pigment dispersion syndrome (PDS) and pigment glaucoma (PG) in the D2 mouse: tyrosinase-related protein 1 gene (*Tyrp1*), which causes iris stromal atrophy, and glycoprotein neuromedin B-associated gene (*Gpnmb*), which is associated with pigment dispersion [15]. The mutations in *Tyrp1* and *Gpnmb* and the phenotypes of PDS and PG from D2 mice segregate among BXD progeny. The BXD strains that harbor mutations in *Tyrp1* and *Gpnmb*, such as BXD55, BXD62, BXD66, etc., develop iris depigmentation [16]. Jablonski's group identified a gene network and modifiers of *Tyrp1* and *Gpnmb* that contribute to phenotypes of PDS and PG using BXD mice and a systems genetics method [16-18]. Currently, BXD lines have been used extensively in genetic and genomic studies of the eye and central visual system to identify the genetic basis of ocular phenotypes, including molecular expression phenotypes and the regulating gene, in our case, the regulation of *Myo7a* expression [17-20].

Mice with a *Myo7a* mutation are deaf and have abnormalities in their RPE [21,22]. There is a *Myo7a* mutation in one BXD parental strain (the D2 mouse), and there is no mutation in the other BXD parental strain (the B6 mouse). We found the expression of *Myo7a* in the retina has significant differences between D2 and B6 mice, which provides an excellent opportunity to study the mechanism through which *Myo7a* causes US by using retina expression data of the BXD population. The purpose of this investigation was to combine the power of BXD RI strains of mice with systems genetics approaches using retinal tissue to identify a genetic network for *Myo7a,* determine the genetic regulation of *Myo7a,* and explore genes functionally related to *Myo7a* and pathways through which *MYO7A* induces US.

METHODS

Mice: A total of 222 mice from 55 strains (52 BXD strains, two parental strains, and their F1 hybrid strain; Appendix 1) were used for this study. During strain selection, we excluded BXD strains that carry the *Tyrp1b* mutation and the *GpnmbR150X* mutation, which result in pigment dispersion glaucoma. We also excluded BXD strains that carry the rd16 mutation and strains that have abnormally high *Gfap* levels previously observed in our retina expression data. Almost all animals were young adults between 60 and 100 days of age balanced for sex. Animals were weaned at 25 days of age and housed in same-sex cages with two to five mice per cage until the day of euthanasia. Animals had free access to standard laboratory chow and water and were maintained on a 12 h:12 h light-dark cycle. Room temperature ranged from 20 to 24 °C.

All experimental protocols were approved by the Institutional Animal Care and Use Committee (IACUC) at the University of Tennessee Health Science Center (Memphis, TN) and Emory University (Atlanta, GA). Mice were handled in a manner consistent with the ARVO Statement for the Use of Animals in Ophthalmic and Vision Research and the Guide for the Care and Use of Laboratory Animals (Institute of Laboratory Animal Resources, the Public Health Service Policy on Humane Care and Use of Laboratory Animals).

Tissue and sample processing: The retinal tissue and RNA were prepared according to our published protocols [23]. Mice were euthanized with rapid cervical dislocation. Two retinas per mouse were immediately removed and immersed in 1 ml of 160 U/ml RiboLock for 1 min at room temperature and then transferred to Hank's Balanced Salt solution with RiboLock in 50 µl RiboLock (RiboLock RNase #EO0381 40 U/µl 2500 U, Thermo Fisher Scientific, Waltham, MA). The RNA was isolated using a QiaCube (QiaGen, Hilden, Germany) and the in-column DNase procedure. The quality and purity of RNA were checked using an Agilent Bioanalyzer 2100 (Agilent Technologies, Santa Clara, CA) system to assess the relative quantities of 18S and 28S RNA, as well as the RNA integrity. The gene expression data were collected using the Affymetrix Mouse Gene 2.0 ST array based on the manufacturer's protocol (Thermo Fisher Scientific). This array was designed with a median of 22 unique probes per transcript that measure gene expression at almost every exon and 3′-untranslated region (UTR) and provide comprehensive transcriptome coverage with more than 30,000 coding and non-coding transcripts.

Quantitative RT–PCR: The expression of *Myo7a* in the retina of the wild-type and mutated BXD mice was verified using quantitative reverse transcription-PCR (qRT-PCR). We performed qRT-PCR as previously described [24]. Briefly, total RNA was extracted from the retinas of the B6, D2, and eight BXD strains (four strains with wild-type and four strains with a mutation at the *Myo7a* gene). Five samples were collected from the B6 mice, five samples were collected from the D2 mice, and three samples were collected from each BXD strain. The total RNA from each individual sample was transcribed into cDNA using the High Capacity cDNA Reverse Transcription Kit (Life Technologies, Carlsbad, CA). Next, a 10-µl PCR reaction mixture was prepared by mixing 4.5 µl of diluted cDNA, 0.25 µl of 10 µM forward primer, 0.25 µl of 10 µM reverse primer and 5 µl 2 × SYBR Green PCR Master Mix (Life Technologies). Quantitative PCR was performed using a StepOne PCR system (Life Technologies) with the following program: 95 °C for 10 min, 40 cycles of 95 °C for 15 s followed by 60 °C for 1 min. At the completion of cycling, melting curve analysis was performed to establish the specificity of the PCR product: 95 °C for 15 s, 60 °C for 1 min and 95 °C for 15 s. *Hprt* (Gene ID 15452, OMIM 308000), a housekeeping gene, was used as an internal control. The primer sequences for mouse transcripts were as follows: *Hprt,* Forward, 5′-GAA AGA CTT GCT CGA GAT GTC ATG-3′, reverse 5′-CAC ACA GAG GGC CAC AAT GT-3′; *Myo7a* forward 5′-CCG CCC AGC AAC ATC CT-3′, reverse 5′-CTT GCG GGA CTG CAG AAA C-3′. The relative expression of the *Myo7a* gene was analyzed with the ΔΔCT method with *Hprt* used as the reference gene for normalization as previously described [24]. Briefly, the threshold cycle (CT) values for *Myo7a* gene was determined by automated threshold analysis using a StepOne Real-Time PCR System and normalized to the CT value of the reference gene Hprt to obtain ΔCT (*Myo7a* gene) = CT(*Myo7a* gene)− CT(Hprt gene). Then *Myo7a* gene expression in each mouse strain relative to that in a reference sample C57BL/6J was calculated as $2^{-\Delta\Delta CT} = 2^{-[\Delta CT(\text{Myo7a gene in each mouse strain}) - \Delta CT(\text{Myo7a gene in C57BL/6J})]}$.

Data processing: Affymetrix CEL files were processed using the Robust Multichip Array (RMA) method and the default set in Affymetrix Expression Console Software [25]. We normalized the RMA expression data using modified Z-scores as previously described [26]. Briefly, we calculated the log base 2 of the RMA values, computed the Z scores for these RMA values for each array, multiplied the Z scores by 2, and added an offset of 8 units to each value. This transformation resulted in a set of Z-like scores for each array with a mean of 8, a variance of 4, and a standard deviation of 2. The advantage of this modified Z score is that a twofold difference in expression corresponds approximately to 1 unit. Finally, we computed the arithmetic mean of the values for the set of microarrays for each strain (an average of four samples per strain), and uploaded this data set into our GeneNetwork (GN) website for future analysis and public access (DoD CDMRP Retina Affy MoGene 2.0 ST (May15) RMA Gene Level).

Heritability calculations: The heritability of the expression level of *Myo7a* was calculated using broad sense heritability that compares the genetic variation between strains to the environmental variance within the strains [27]. The formula used for the heritability calculation was 0.5 Vg / (0.5 Vg + Ve), where Vg is the genetic variance (variances of the strain means), and Ve is the environmental variance. The factor of 0.5 in this ratio was applied to adjust for the twofold increase in the additive genetic variance among the inbred strains relative to the outbred populations [20].

eQTL mapping and SNP analysis: Expression quantitative trait locus (eQTL) mapping was performed using the WebQTL module on GeneNetwork using our published methods [23, 26,28]. This methodology uses regression analysis to determine the relationship between differences in a trait and differences in alleles at markers across the genome. Simple interval mapping was performed to identify potential eQTLs that regulate *Myo7a* expression levels and estimate the significance at each location using known genotype data for those sites. Composite interval mapping was also performed to control for genetic variance associated with major eQTLs and therefore identify any secondary eQTLs that may have been otherwise masked. Each analysis produced a likelihood ratio statistic (LRS) score, providing us with a quantitative measure of confidence of linkage between the observed phenotype—in this case, variation in expression level of *Myo7a*—and known genetic markers. The genome-wide significance for each eQTL was established using a permutation test that compared the LRS of our novel site with the LRS values for 1,000–10,000 genetic permutations [29]. Sequence variability between B6 and D2 was determined using the single nucleotide polymorphism (SNP) variant browser link on GeneNetwork.

Genetic correlation and partial correlation analysis: We computed the Pearson product–moment correlations of the strain means between the expression of *Myo7a* and the expression of all the other probe sets across the mouse genome to produce sets of genetically correlated genes. To identify true biologic correlates of *Myo7a*, we also performed partial correlation analyses to remove linkage disequilibrium by controlling genetic variation near *Myo7a* (locus rs8281437 at 105.2 Mb of chromosome 7). Then we performed a literature correlation to rank the list of genes using the Semantic Gene Organizer (SGO) software that automatically extracts

gene–gene relations from titles and abstracts in MEDLINE citations [30]. All genetic correlations, partial correlations, and literature correlations were computed using the tools on GeneNetwork.

Gene set enrichment analysis and gene network construction: Genes with a statistically significant genetic correlation and a partial correlation with *Myo7a* were selected and uploaded to Webgestalt for gene enrichment analysis [31]. The p values generated from the hypergeometric test were automatically adjusted to account for multiple comparisons using the Benjamini and Hochberg correction [32]. The categories with an adjusted p value (adj P) of less than 0.05 indicated that the set of submitted genes is statistically significantly over-represented in those categories.

The gene network was constructed and visualized using the Cytoscape utility through the Gene-set Cohesion Analysis Tool (GCAT). Nodes in the network represent genes, and edges between two nodes represent the cosine score of latent semantic indexing (LSI) that determines the functional coherence of gene sets is larger than 0.6. The significance of the functional cohesion is evaluated by the observed number of gene relationships above a cosine threshold of 0.6 in the LSI model. The literature p value (LP) is calculated using Fisher's exact test by comparing the cohesion of the given gene set to a random gene set [30].

RESULTS

Myo7a expression levels in the retinas of B6, D2, and BXD mice, and heritability: There was a high level of variation in the expression level of *Myo7a* among the BXD strains. The average expression level of *Myo7a* in all BXD strains was 8.69±0.09 (mean ± SE). The range included a high of 9.63±0.06 for BXD6 and a low of 7.69±0.02 for BXD84 (Figure 1), a more than 3.8-fold change among the BXD strains. In the B6 parental strain, *Myo7a* had an average expression level of 9.22±0.02. In the D2 parental strain, *Myo7a* had an average expression level of 7.92±0.09. There was statistically significant difference in the expression of *Myo7a* between B6 and D2 ($p<0.01$). Similarly, BXD lines with the B6 allele at the *Myo7a* locus had higher *Myo7a* expression levels while those with the D2 allele at the *Myo7a* locus had lower expression levels (9.12±0.38 and 7.92±0.31, respectively; $p<0.0001$; Figure 2). To validate *Myo7a* expression from the array, we performed quantitative RT–PCR for the B6, D2, and 8 BXD strains (four strains with wild-type (BXD16, 43, 65b, and 29) and four strains with a mutation in the *Myo7a* gene (BXD86, 60, 87, and 09)). This analysis confirmed the statistically significant difference in the expression of *Myo7a* between the B6 and D2 mice and between the B6 allele and the D2 allele at the *Myo7a* locus among the BXD strains ($p<0.0001$; Figure 3). The heritability of *Myo7a* expression levels was 0.83, which suggested that a genetic factor is a major contributor to variation in expression. This heritable variation enables us to identify a genetic locus that controls the expression levels of *Myo7a* in BXD mice.

eQTL mapping and sequence variants of Myo7a: Simple interval mapping for *Myo7a* revealed a highly significant eQTL with an LRS of 86.1 at chromosome 7, the location of the gene itself (Figure 4). Composite interval mapping revealed no secondary loci that modulate *Myo7a* expression levels. Thus, *Myo7a* is defined as *cis*-regulated eQTL, suggesting the variation in the transcript expression levels is caused by sequence variants in or near *Myo7a*. We found a total of 764 SNPs in *Myo7a* between the BXD parental strains using new open access sequence data resources at GeneNetwork, which include all of the current available sequence variances of BXD mice. Most of those SNPs are located in introns. Three are located in the 3′-UTR or 5′-UTR. Thirty-four SNPs are located at coding areas, three of which are non-synonymous SNPs (Table 1). All SNPs located at the UTR and coding areas are listed in Appendix 2.

Gene function enrichment: The 1,569 probe sets found to correlate significantly with *Myo7a* expression after genetic and partial correlations ($p<0.05$) were uploaded to Webgestalt. Among them, 495 probe sets were mapped to multiple Entrez gene ID or could not be mapped to any Entrez gene ID, resulting in 1,074 probe sets that can unambiguously map to 1,048 unique Entrez gene IDs. These probe sets were then used for enrichment analysis. The most significant enrichments in the molecular function category are "cation channel activity," "metal ion transmembrane transporter activity," "voltage-gated channel activity," and "gated channel activity" (Appendix 3). The most significant enrichments in the biologic process category are "ion transmembrane transport," "ion transport," "membrane repolarization," and "regulation of ion transmembrane transport" (Appendix 4). The most significant enrichments in the cellular component category are "axon part," "cell periphery," "plasma membrane," "dendrite," and "neuron projection" (Appendix 5). Gene pathway analysis showed that the genes are significantly enriched in "Calcium signaling," "Neuroactive ligand-receptor interaction," "Chemokine signaling," and "Axon guidance" pathways (Table 2).

Genetic network: The strength of correlation among genes with which *Myo7a* is correlated can be evaluated using a coexpression network. To identify known biologic relations among coexpressed genes, we performed a literature correlation analysis after the genetic and partial correlation analysis.

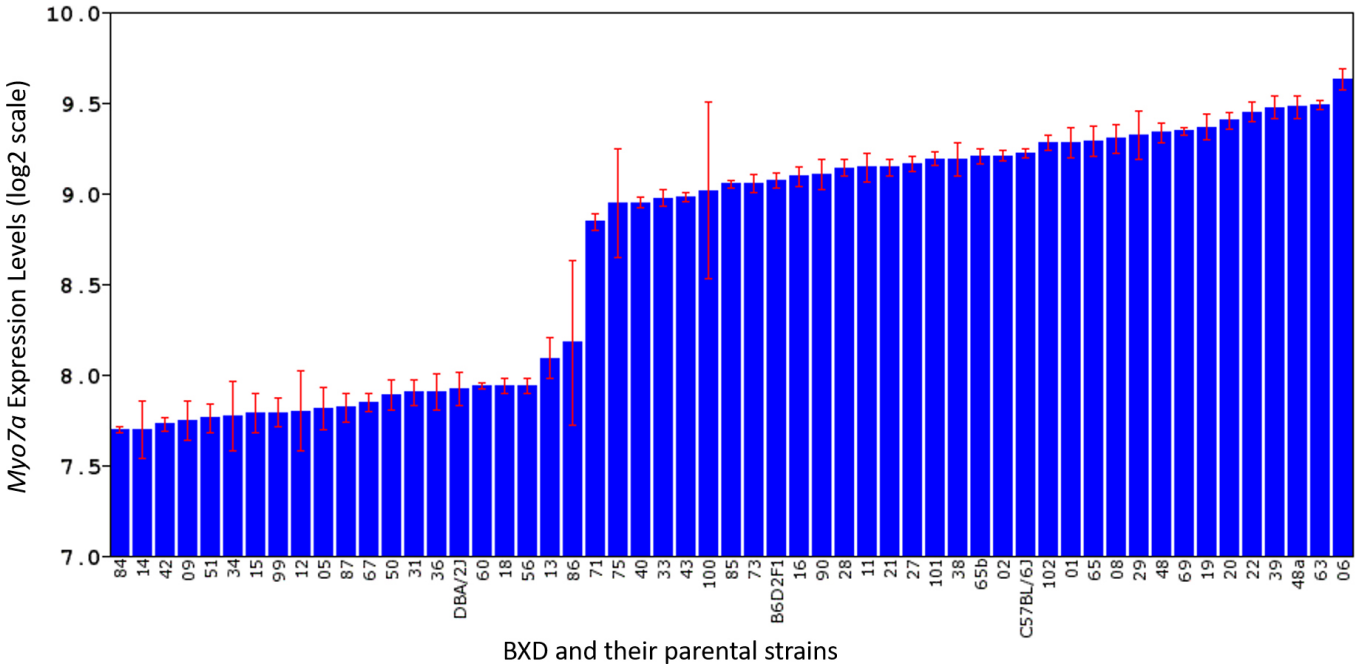

Figure 1. Expression of *Myo7a* in the retina for the B6 and D2 parental strains, F1 hybrids, and 52 BXD lines. Expression for each strain (four mice per strain) was generated using the RMA method and the Affymetrix Expression Console Software and normalized using modified Z-scores. The x-axis denotes the strain while the y-axis denotes the mean expression given in a log2 scale. Each bar shows the mean expression values ± standard error of the mean (SEM).

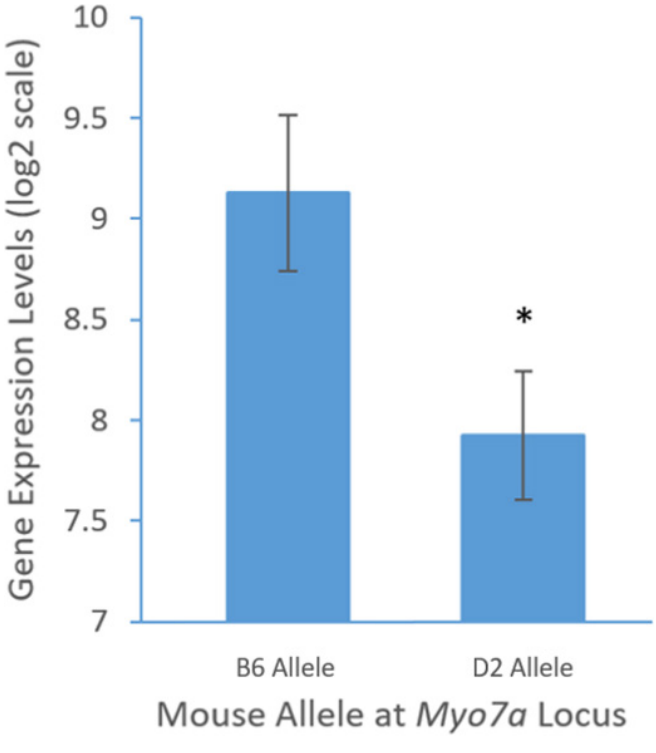

Figure 2. The mean expression of *Myo7a* of BXD strains with the B allele and the D allele at the *Myo7a* locus. Among the 55 strains used, 33 have the B allele at the *Myo7a* locus, 19 have the D allele, and three are heterozygous. The values on the y-axis denote normalized expression levels on a log2 scale. There is a statistically significant difference in the expression of *Myo7a* among the strains carrying the B versus D alleles ($p<0.0001$).

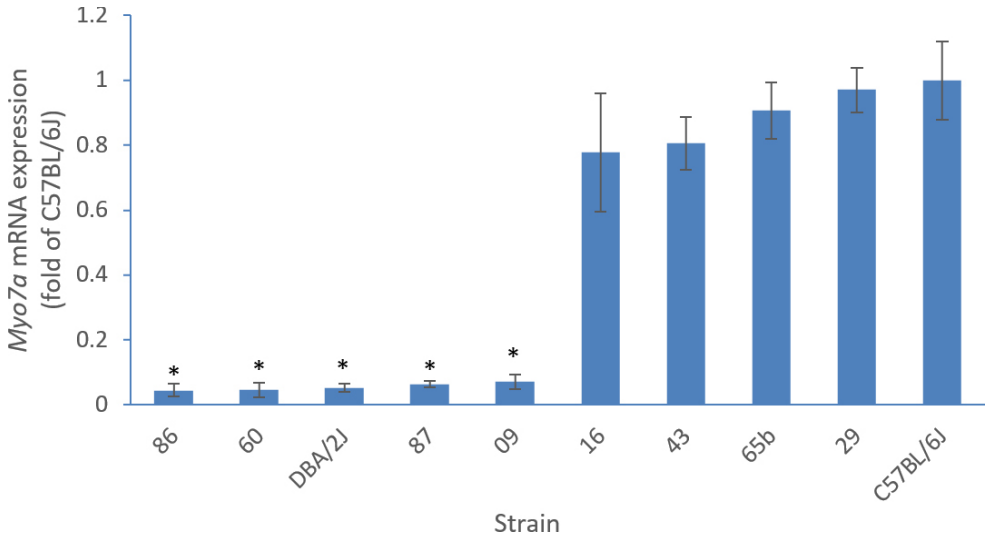

Figure 3. mRNA expression of *Myo7a* in the retina for the B6 and D2 strains and eight selected BXD lines. The x-axis denotes the strain while the y-axis denotes the fold change in the *Myo7a* gene for the nine strains relative to the B6 strain using the ΔΔcT method. Each bar shows the mean relative expression values ± standard error of the mean (SEM). n=3–5; p<0.0001.

The top 50 genes (literature correlation coefficient >0.37) were uploaded to GCAT for functional coherence analysis and gene network construction. Five genes could not be found in the GCAT database, four genes had no functional relationship with the other genes in the network, and one gene was a Riken clone. These ten genes were excluded from the gene coherence analysis. The remaining 40 genes (Appendix 6) showed significant functional cohesion with a literature p value of 1.693507e-17 (Figure 5). Multiple resources, including Chillibot, GeneCards, and PubMed, were used to determine

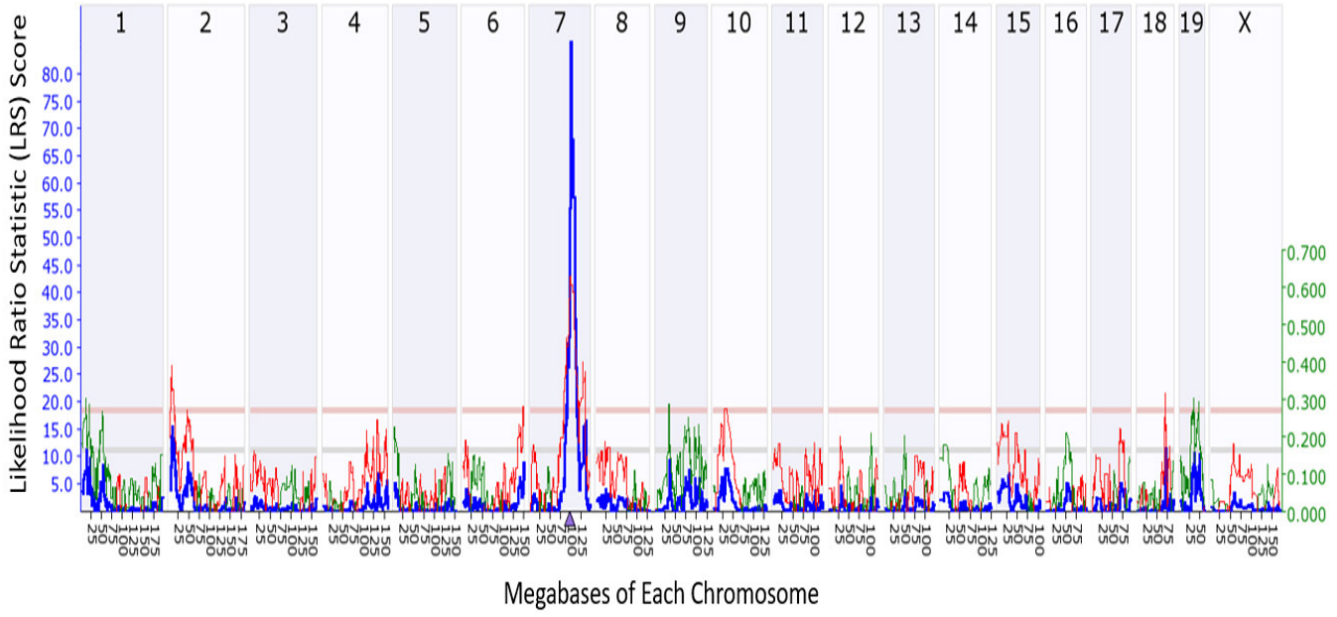

Figure 4. Genetic mapping of *Myo7a*. A statistically significant expression quantitative trait locus (eQTL) is present at the location of *Myo7a* itself (the triangle on the x-axis) on chromosome 7, making it a *cis*-eQTL. The left y-axis provides the likelihood ratio statistic (LRS) score in blue, and the right y-axis provides the additive effect. The red and green lines show the effect of the D or B allele on trait values, respectively. The upper x-axis shows the location by chromosome, and the lower x-axis shows the location in megabases. The two horizontal lines across the plot make the threshold for genome-wide statistically significant (p<0.05, red or upper line) and suggestive (p<0.63, gray or lower line) thresholds.

Table 1. Nonsynonymous SNPs that are located within *Myo7a* gene.

SNP ID	Chr	Mb	Alleles	Domain	Function	B6	D2
wt37–7-105239564	7	105.2396	T/C	Exon 14	Nonsynonymous	T	C
wt37–7-105246235	7	105.2462	C/T	Exon 6	Nonsynonymous	C	T
wt37–7-105255574	7	105.2556	A/G	Exon 3	Nonsynonymous	A	G

Table 2. The significant enriched KEGG pathway.

Pathway Name	N of genes	adjusted P Value
Calcium signaling pathway	20	0.0092
Neuroactive ligand-receptor interaction	26	0.0129
Chemokine signaling pathway	19	0.0129
Axon guidance	14	0.0387

whether members of the *Myo7a* coexpression network had been previously associated with retinitis pigmentosa or deafness, the main symptoms of US. In addition to *Myo7a*, some genes in this network (*Fzd4*, *Sema4a*, *Trex1*, *Sumf1*, *Trim32*, and *Ccdc28b*) are already known to be related to retinitis pigmentosa or other retinal diseases. Several genes (*Fgf3*, *Psap*, and *Ank1*) are related to deafness. Furthermore, some genes in the network (*Ank1*, *Ddr1*, *Neb*, *Numbl*, and *Sema4a*) share the same transcription factor (AP4) with *Myo7a*.

DISCUSSION

We analyzed the differential expression of *Myo7a* in the retinal tissue of BXD RI mice and found *Myo7a* to be *cis*-regulated, indicating that it is regulated by itself or genes close to it. We present a genetic network for *Myo7a* that

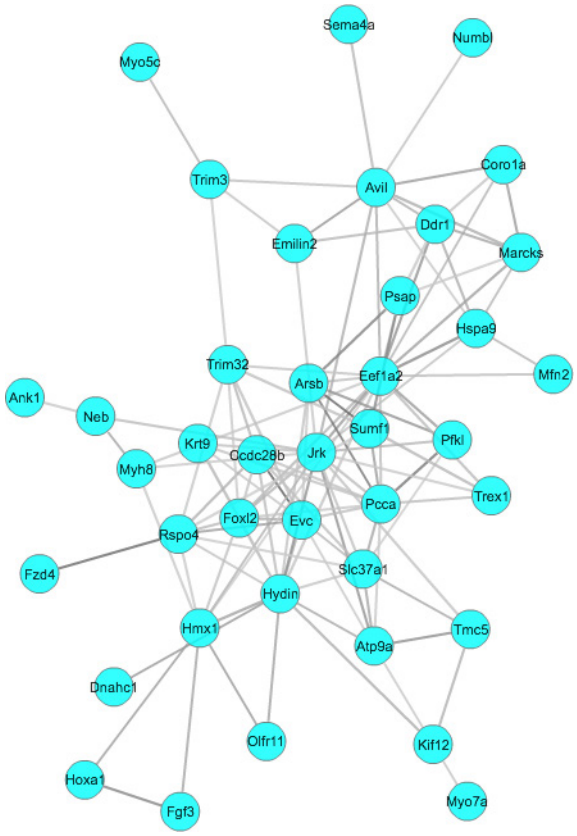

Figure 5. *Myo7a* gene network graph created using the Gene-set Cohesion Analysis Tool described in the Methods section. These genes may be functionally related. Gene symbols are located at nodes in circles, and the lines interconnecting the nodes are based on literature correlations. The literature p value for these genes is 1.693507e-17. This computation was based on the 40 terms that most frequently co-occur with *Myo7a*.

involves genes that we found were related to retinal diseases and deafness via literature reports. Finally, we present gene enrichment categories and pathways through which *Myo7a* and its genetic network interact to affect US phenotypes.

We created a genetic network using the top 40 correlated genes with *Myo7a*. In this network, *Fzd4, Sema4a, Trex1, Sumf1, Trim32,* and *Ccdc28b* are known to be associated with retinal diseases. We propose that these genes could interact with *Myo7a* to affect the severity of US.

Retinitis pigmentosa is a highly heterogeneous disease characterized by degeneration of rod photoreceptors and often presents with night blindness, progressive peripheral visual field loss, and blindness [33]. US and Bardet-Biedl syndrome present with retinitis pigmentosa. US and Bardet-Biedl syndrome account for 1,200 pathogenic mutations out of 3,100 mutations in more than 50 genes known to cause non-syndromic RP [34]. From the gene network we constructed, *Trim32* and *Ccdc28B* are key players in Bardet-Biedl syndrome and may also play a part in the presentation of the severity of RP in US. Tripartite motif-containing protein 32 (*Trim32*) is known to cause Bardet-Biedl syndrome, an autosomal recessive disorder characterized by vision loss due to retinal tissue degeneration, obesity, polydactyly, and mental retardation [35]. Coiled-coil domain-containing protein 28B (*Ccdc28B*) colocalizes and interacts with several proteins involved with Bardet-Biedl syndrome [36]. *Ccdc28B* is a modifier gene, meaning that a hypomorphic mutation in *Ccdc28B* affects the expressivity of Bardet-Biedl syndrome, but in itself the gene is not a cause of the syndrome [37].

Semaphorin-4a (*Sema4a*) is a transmembrane protein that plays a role in retinal development [36,38]. *Sema4a* participates in cell–cell communication in the immune system and is present in the brain and eye. It is mainly found in the RPE and the inner retina when the photoreceptor outer segments lengthen. Mice with *Sema4a* deficiency have been shown to have compromised function of rod and cone photoreceptors, as well as severe retinal degeneration, thinner retinal vessels, and depigmentation using fundus photography [39]. *Sema4a* is also implicated in cone rod dystrophy [40].

Three more genes from the network (*Fzd4, Trex1,* and *Sumf1*) are also reported to be involved in retinal diseases. Frizzled-4, or *Fzd4*, has been linked to familial exudative vitreoretinopathy (FEVR) which, similar to retinitis pigmentosa, is a hereditary vitreoretinal disorder that affects the blood vessels in the eye and can lead to blindness [41,42].

Three prime repair exonuclease 1 (*Trex1*) is a 3′-5′ exonuclease that affects the vasculature of the retina. Retinal vasculopathy with cerebral leukodystrophy (RVCL) is a genetic condition affecting the central nervous system that leads to loss of vision, strokes, and dementia, and is caused by mutations in the *TREX1* (Gene ID 11277, OMIM 606609) gene [43]. Ophthalmologic findings show capillary dropouts leading to loss of central vision, prominent juxtafoveolar capillary obliteration, and telangiectasis, as well as transient ischemic strokes, cognitive dysfunction, and personality disorders [44].

Mutations in sulfatase-modifying factor 1 (*Sumf1*) are the primary cause of multiple sulfatase deficiency (MSD), which is a metabolic abnormality featuring a reduction in several sulfatase functions. MSD is often characterized by neurodegeneration, coarse facial features, nystagmus, and neuropathy [45]. MSD also often occurs with eye abnormalities, such as retinal degeneration [46]. Furthermore, *SUMF1* (Gene ID 285362, OMIM 607939) activates arylsulfatase I (*ARSI*; Gene ID 340075, OMIM 610009), which is preferentially expressed in the human RPE cell line ARPE-19 and is a candidate gene for affecting inherited eye diseases [47].

All of these genes are associated with retinal pathology and are good candidates for explaining the variety of ocular symptoms not only between US subtypes but also within each type. However, further investigation is needed to elucidate the relationship between each gene and *Myo7a*.

Although other genes in the *Myo7a* gene network have not been reported to be involved in retinal diseases thus far, they could be novel genes that work with *Myo7a* to affect symptom severity of US, especially genes that have been regulated by the same transcription factor as *Myo7a*. The transcription binding site analysis showed AP4 to regulate *Myo7a* along with *Ank1*, *Ddr1*, *Neb*, *Numbl*, and *Sema4a*.

Replication initiator 1 (*Repin1*), also known as AP4, is a transcription factor that binds the promoter sites of *Myo7a, Ddr1, Numbl, Sema4a, Neb,* and *Ank1*. As discussed earlier, *Sema4a* is related to retinal development, and defects in Ankyrin 1 (*Ank1*) are implicated in hearing loss [47,48]. Discoidin domain receptor family, member 1 (*Ddr1*) is involved in the regulation of cell growth, differentiation, and metabolism. Deletion of the *Ddr1* gene is associated with a severe decrease in auditory function, and *Ddr1* mutant mice have alterations in the organ of Corti [49]. *Ddr1* also lies near several deafness loci linked to autosomal recessive or dominant non-syndromic hearing loss [50,51]. Numb-like protein, or *Numbl*, is expressed in the rat auditory sensory epithelium [52]. Nebulin, or *Neb*, is an actin-binding protein that promotes the contractile function of sarcomeres. A non-synonymous variant of *Neb* may be involved in glaucoma, characterized by degeneration of retinal ganglion cells, in basset hounds [53]. Because *Repin1* is the transcription factor

for these genes, each of which is related to either the retina or hearing, it may also play a role in deaf-blindness, although there are not many previous studies linking *Repin1* to either symptom.

Gene enrichment analysis was used to identify gene ontology (GO) categories in which *Myo7a* and its correlated genes were over-represented and the pathways through which they interact. Many of the enrichment categories in molecular function and biologic process that were over-represented were related to transmembrane ion channel activity, and the most significant enrichments in cellular components were neuron-specific. Furthermore, one pathway revealed to be significant in the present pathway analysis was "neuroactive ligand-receptor interaction" and "axon guidance." This is not surprising, because hearing involves transmitting sound vibrations to the cochlear and vestibular labyrinths, where mechanoelectrical transduction carries neural signals for integration, processing, and feedback. *Myo7a* is responsible for unconventional myosin found in stereocilia. Stereocilia contain tip links, thought to be mechanical springs needed to open the ion channels leading to depolarization [54]. Single hair cell measurements of mice with mutations in *Myo7a* have shown that when the stereocilia are not stimulated by sound, the gating springs are slack and transduction channels closed, as opposed to a maintained tension on the gating springs that keep some of the channels open even at rest in normal hair cells. Transducer currents can be measured in these mutant mice, which reflects cation flow into hair cells through transduction channels, but only with strong deflection of stereocilia bundles [55]. *Myo7a* is heavily implicated in the hair cells and transduction channels in the ear.

Gene pathway analysis further revealed "calcium signaling" to be a significant pathway in *Myo7a* interactions, supported by our GO analysis category "cation channel activity." *Myo7a* has been reported to be a Ca^{2+}/calmodulin-regulated gene and has altered expression when Ca^{2+} homeostasis was altered. Since *Myo7a* is expressed in rods and cones, changes in its expression may reflect differences in Ca^{2+} homeostasis in rods versus cones [56]. Although the exact nature of how *Myo7a* interacts with calcium signaling is still not clear, our gene ontology results support our pathway findings.

These gene ontology and pathways presented imply that many of *Myo7a*'s interactions with correlated genes are involved in ion channel activity, as well as neurons. Further investigation is needed to elucidate the exact nature of these relationships, and how *Myo7a*, its genetic network, and pathways all interact to affect the severity of expression of US.

Conclusion: The expression of US is highly variable, and symptoms that manifest may differ in severity, even within the same US category. *Myo7a* is a causal gene of US type I, but many other factors interact with this gene to modify disease severity. Here, we propose a gene network, gene ontology categories, and pathways that interact with *Myo7a*. We found several genes in the genetic network to be related to deafness and blindness, and several others shared the same transcript factor with *Myo7a*. We further examined these relationships using gene ontology and pathway analysis and found that many of these genes interact with ion channel activity and neuronal activity, which is crucial in vision and hearing. Further investigation is needed to elucidate the nature and mechanisms of these relationships, which may assist in the treatment of symptoms of US.

APPENDIX 1. THE LIST OF STRAINS WITH LOG2 TRANSFERRED EXPRESSION VALUE OF MYO7A IN RETINA.

To access the data, click or select the words "Appendix 1"

APPENDIX 2. SNPS THAT ARE LOCATED UTR AND CODING REGIONS WITHIN MYO7A GENE.

To access the data, click or select the words "Appendix 2"

APPENDIX 3. THE SIGNIFICANT ENRICHMENTS IN MOLECULAR FUNCTION CATEGORY.

To access the data, click or select the words "Appendix 3"

APPENDIX 4. THE SIGNIFICANT ENRICHMENTS IN BIOLOGICAL PROCESS CATEGORY.

To access the data, click or select the words "Appendix 4"

APPENDIX 5. THE SIGNIFICANT ENRICHMENTS IN CELLULAR COMPONENT CATEGORY.

To access the data, click or select the words "Appendix 5"

APPENDIX 6. THE LIST OF GENES THAT ARE USED TO CONSTRUCT MYO7A GENE NETWORK.

To access the data, click or select the words "Appendix 6"

ACKNOWLEDGMENTS

This work was supported by NIH Grant R01EY021200 (LL, PI), NIH grant R01EY017841 (EEG, PI), NIH grants R01EY022694 and R01EY026629 (WZ, PI), DoD Grant W81XWH-12–1-0255 (EEG, PI), Research to Prevent Blindness Stein Innovation Award (Robert Williams, PI), and

Vision Core Grant P30EY006360 (P. Michael Iuvone, PI). This study was supported in part by the Emory Integrated Genomics Core (EIGC), which is subsidized by the Emory University School of Medicine and is one of the Emory Integrated Core Facilities. We thank Dr. Robert Williams for his financial and bioinformatics support for this study.

REFERENCES

1. Gibbs D, Kitamoto J, Williams D. Abnormal phagocytosis by retinal pigmented epithelium that lacks myosin VIIa, the Usher syndrome 1B protein. Proc Natl Acad Sci USA 2003; 100:6481-6. [PMID: 12743369].

2. Bharadwaj AK, Kasztejna JP, Huq S, Berson EL, Dryja TP. Evaluation of the myosin VIIA gene and visual function in patients with Usher syndrome type I. Exp Eye Res 2000; 71:173-81. [PMID: 10930322].

3. Ouyang XM, Yan D, Du LL, Hejtmancik JF, Jacobson SG, Nance WE, Li AR, Angeli S, Kaiser M, Newton V, Brown SD, Balkany T, Liu XZ. Characterization of Usher syndrome type I gene mutations in an Usher syndrome patient population. Hum Genet 2005; 116:292-9. [PMID: 15660226].

4. Jaijo T, Aller E, Oltra S, Beneyto M, Najera C, Ayuso C, Baiget M, Carballo M, Antinolo G, Valverde D, Moreno F, Vilela C, Perez-Garrigues H, Navea A, Millan JM. Mutation profile of the MYO7A gene in Spanish patients with Usher syndrome type I. Hum Mutat 2006; 27:290-1. [PMID: 16470552].

5. Roux AF, Faugere V, Le Guedard S, Pallares-Ruiz N, Vielle A, Chambert S, Marlin S, Hamel C, Gilbert B, Malcolm S, Claustres M. French Usher Syndrome C. Survey of the frequency of USH1 gene mutations in a cohort of Usher patients shows the importance of cadherin 23 and protocadherin 15 genes and establishes a detection rate of above 90%. J Med Genet 2006; 43:763-8. [PMID: 16679490].

6. Oshima A, Jaijo T, Aller E, Millan JM, Carney C, Usami S, Moller C, Kimberling WJ. Mutation profile of the CDH23 gene in 56 probands with Usher syndrome type I. Hum Mutat 2008; 29:E37-46. [PMID: 18429043].

7. Bonnet C, Riahi Z, Chantot-Bastaraud S, Smagghe L, Letexier M, Marcaillou C, Lefevre GM, Hardelin JP, El-Amraoui A, Singh-Estivalet A, Mohand-Said S, Kohl S, Kurtenbach A, Sliesoraityte I, Zobor D, Gherbi S, Testa F, Simonelli F, Banfi S, Fakin A, Glavac D, Jarc-Vidmar M, Zupan A, Battelino S, Martorell Sampol L, Claveria MA, Catala Mora J, Dad S, Moller LB, Rodriguez Jorge J, Hawlina M, Auricchio A, Sahel JA, Marlin S, Zrenner E, Audo I, Petit C. An innovative strategy for the molecular diagnosis of Usher syndrome identifies causal biallelic mutations in 93% of European patients. Eur J Hum Genet 2016; 24:1730-8. [PMID: 27460420].

8. Dad S, Rendtorff ND, Tranebjaerg L, Gronskov K, Karstensen HG, Brox V, Nilssen O, Roux AF, Rosenberg T, Jensen H, Moller LB. Usher syndrome in Denmark: mutation spectrum and some clinical observations. Mol Genet Genomic Med 2016; 4:527-39. [PMID: 27957503].

9. Rong W, Chen X, Zhao K, Liu Y, Liu X, Ha S, Liu W, Kang X, Sheng X, Zhao C. Novel and recurrent MYO7A mutations in Usher syndrome type 1 and type 2. PLoS One 2014; 9:e97808-</jrn>[PMID: 24831256].

10. Liu XZ, Hope C, Walsh J, Newton V, Ke XM, Liang CY, Xu LR, Zhou JM, Trump D, Steel KP, Bundey S, Brown SD. Mutations in the myosin VIIA gene cause a wide phenotypic spectrum, including atypical Usher syndrome. Am J Hum Genet 1998; 63:909-12. [PMID: 9718356].

11. Jacobson SG, Cideciyan AV, Gibbs D, Sumaroka A, Roman AJ, Aleman TS, Schwartz SB, Olivares MB, Russell RC, Steinberg JD, Kenna MA, Kimberling WJ, Rehm HL, Williams DS. Retinal disease course in Usher syndrome 1B due to MYO7A mutations. Invest Ophthalmol Vis Sci 2011; 52:7924-36. [PMID: 21873662].

12. Kallman JC, Phillips JO, Bramhall NF, Kelly JP, Street VA. In search of the DFNA11 myosin VIIA low- and mid-frequency auditory genetic modifier. Otol Neurotol 2008; 29:860-7. [PMID: 18667942].

13. Street VA, Li J, Robbins CA, Kallman JC. A DNA variant within the MYO7A promoter regulates YY1 transcription factor binding and gene expression serving as a potential dominant DFNA11 auditory genetic modifier. J Biol Chem 2011; 286:15278-86. [PMID: 21378158].

14. John SW, Smith RS, Savinova OV, Hawes NL, Chang B, Turnbull D, Davisson M, Roderick TH, Heckenlively JR. Essential iris atrophy, pgment dispersion, and glaucoma in DBA/2J mice. Invest Ophthalmol Vis Sci 1998; 39:951-62. [PMID: 9579474].

15. Anderson MG, Smith RS, Hawes NL, Zabaleta A, Chang B, Wiggs JL, John SW. Mutations in genes encoding melanosomal proteins cause pigmentary glaucoma in DBA/2J mice. Nat Genet 2002; 30:81-5. [PMID: 11743578].

16. Swaminathan S, Lu H, Williams RW, Lu L, Jablonski MM. Genetic Modulation of the Iris Transillumination Defect: A Systems Genetics Analysis Using the Expanded Family of BXD Glaucoma Strains. Pigment Cell Melanoma Res 2013; 26:487-98. [PMID: 23582180].

17. Lu H, Watson ER, Williams RW, Geisert EE, Jablonski MM, Lu L. Complex interactions of Tyrp1 in the eye. Mol Vis 2011; 17:2455-68. [PMID: 21976956].

18. Lu H, Wang X, Pullen M, Guan H, Chen H, Sahu S, Zhang B, Chen H, Williams RW, Geisert EE, Lu L, Jablonski MM. Invest Ophthalmol Vis Sci 2011; 52:4132-42. [PMID: 21398278].

19. Templeton JP, Nassr M, Vazquez-Chona F, Freeman-Anderson NE, Orr WE, Williams RW, Geisert EE. Differential response of C57BL/6J mouse and DBA/2J mouse to optic nerve crush. BMC Neurosci 2009; •••:10-[PMID: 19643015].

20. Geisert EE, Lu L, Freeman-Anderson NE, Templeton JP, Nassr M, Wang X, Gu W, Jiao Y, Williams RW. Gene expression in the mouse eye: an online resource for genetics using 103 strains of mice. Mol Vis 2009; 15:1730-63. [PMID: 19727342].

21. Gibbs D, Diemer T, Khanobdee K, Hu J, Bok D, Williams DS. Function of MYO7A in the Human RPE and the Validity of Shaker1 Mice as a Model for Usher Syndrome 1B. Invest Ophthalmol Vis Sci 2010; 51:1130-5. [PMID: 19643958].

22. Libby RT, Steel KP. Electroretinographic anomalies in mice with mutations in Myo7a, the gene involved in human Usher syndrome type 1B. Invest Ophthalmol Vis Sci 2001; 42:770-8. [PMID: 11222540].

23. King R, Lu L, Williams RW, Geisert EE. Transcriptome networks in the mouse retina: An exon level BXD RI database. Mol Vis 2015; 21:1235-51. [PMID: 26604663].

24. Zhu S, Liu H, Sha H, Qi L, Gao DS, Zhang W. PERK and XBP1 differentially regulate CXCL10 and CCL2 production. Exp Eye Res 2017; 155:1-14. .

25. Bolstad BM, Irizarry RA, Astrand M, Speed TP. A comparison of normalization methods for high density oligonucleotide array data based on variance and bias. Bioinformatics 2003; 19:185-93. .

26. Chesler EJ, Lu L, Shou S, Qu Y, Gu J, Wang J, Hsu HC, Mountz JD, Baldwin NE, Langston MA, Threadgill DW, Manly KF, Williams RW. Complex trait analysis of gene expression uncovers polygenic and pleiotropic networks that modulate nervous system function. Nat Genet 2005; 37:233-42. [PMID: 15711545].

27. Hegmann JP, Possidente B. Estimating genetic correlations from inbred strains. Behav Genet 1981; 11:103-14. [PMID: 7271677].

28. Lu H, Lu L, Williams RW, Jablonski MM. Iris transillumination defect and its gene modulators do not correlate with intraocular pressure in the BXD family of mice. Mol Vis 2016; 22:224-33. [PMID: 27011731].

29. Churchill GA, Doerge RW. Empirical Threshold Values for Quantitative Trait Mapping. Genetics 1994; 138:963-71. [PMID: 7851788].

30. Homayouni R, Heinrich K, Wei L, Berry MW. Gene clustering by latent semantic indexing of MEDLINE abstracts. Bioinformatics 2005; 21:104-15. [PMID: 15308538].

31. Zhang B, Kirov S, Snoddy J. WebGestalt: an integrated system for exploring gene sets in various biological contexts. Nucleic Acids Res 2005; 33:W741–8-[PMID: 15980575].

32. Benjamini Y, Hochberg Y. Controlling the False Discovery Rate: A Practical and Powerful Approach to Multiple Testing. J R Stat Soc Ser A Stat Soc 1995; 57:289-300. .

33. Ayuso C, Millan JM. Retinitis pigmentosa and allied conditions today: a paradigm of translational research. Genome Med 2010; 2:34-[PMID: 20519033].

34. Daiger SP, Sullivan LS, Bowne SJ. Genes and mutations causing retinitis pigmentosa. Clin Genet 2013; 84:132-41. [PMID: 23701314].

35. Kwitek-Black AE, Carmi R, Duyk GM, Buetow KH, Elbedour K, Parvari R, Yandava CN, Stone EM, Sheffield VC. Linkage of Bardet-Biedl syndrome to chromosome 16q and evidence for non-allelic genetic heterogeneity. Nat Genet 1993; 5:392-6. [PMID: 8298649].

36. Badano JL, Leitch CC, Ansley SJ, May-Simera H, Lawson S, Lewis RA, Beales PL, Dietz HC, Fisher S, Katsanis N. Dissection of epistasis in oligogenic Bardet-Biedl syndrome. Nature 2006; 439:326-30. [PMID: 16327777].

37. Liu Q, Saveliev A, Pierce EA. The Severity of Retinal Degeneration in Rp1h Gene-Targeted Mice is Dependent on Genetic Background. Invest Ophthalmol Vis Sci 2009; 50:1566-74. [PMID: 19060274].

38. Ayuso C, Millan JM. Retinitis pigmentosa and allied conditions today: a paradigm of translational research. Genome Med 2010; •••:38-[PMID: 20519033].

39. Rice DS, Huang W, Jones HA, Hansen G, Ye GL, Xu N, Wilson EA, Troughton K, Vaddi K, Newton RC, Zambrowicz BP, Snads AT. Severe retinal degeneration associated with disruption of semaphoring 4A. Invest Ophthalmol Vis Sci 2004; 45:2767-77. [PMID: 15277503].

40. Abid A, Ismail M, Mehdi SQ. Identification of novel mutations in the SEMA4A gene associated with retinal degenerative diseases. J Med Genet 2006; 43:378-81. [PMID: 16199541].

41. Kondo H, Hayashi H, Oshima K, Tahira T, Hayashi K. Frizzled 4 gene (FZD4) mutations in patients with familial exudative vitreoretinopathy with variable expressivity. Br J Ophthalmol 2003; 87:1291-5. [PMID: 14507768].

42. Robitaille J, MacDonald ML, Kaykas A, Sheldahl LC, Zeisler J, Dubé MP, Zhang LH, Singaraja RR, Guernsey DL, Zheng B, Siebert LF, Hoskin-Mott A, Trese MT, Pimstone SN, Shastry BS, Moon RT, Hayden MR, Goldberg YP, Samuels ME. Mutant frizzled-4 disrupts retinal angiogenesis in familial exudative vitreoretinopathy. Nat Genet 2002; 32:326-30. [PMID: 12172548].

43. Richards A, van den Maagdenberg AM, Jen JC, Kavanagh D, Bertram P, Spitzer D, Liszewski MK, Barilla-Labarca ML, Terwindt GM, Kasai Y, McLellan M, Grand MG, Vanmolkot KR, de Vries B, Wan J, Kane MJ, Mamsa H, Schäfer R, Stam AH, Haan J, de Jong PT, Storimans CW, van Schooneveld MJ, Oosterhuis JA, Gschwendter A, Dichgans M, Kotschet KE, Hodgkinson S, Hardy TA, Delatycki MB, Hajj-Ali RA, Kothari PH, Nelson SF, Frants RR, Baloh RW, Ferrari MD, Atkinson JP. C-terminal truncations in human 3′-5′ DNA exonuclease TREX1 cause autosomal dominant retinal vasculopathy with cerebral leukodystrophy. Nat Genet 2007; 39:1068-70. [PMID: 17660820].

44. Kavanagh D, Spitzer D, Kothari P, Aisha S, Liszewski MK, Richards A, Atkinson JP. New roles for the major human 3′-5′ exonuclease TREX1 in human disease. Cell Cycle 2008; 7:1718-25. [PMID: 18583934].

45. Prasad C, Rupar CA, Campbell C, Napier M, Ramsay D, Tay KY, Sharan S, Prasad AN. Case of Multiple Sulfatase Deficiency and Ocular Albinism: A Diagnostic Odyssey. Can J Neurol Sci 2014; 41:626-31. [PMID: 25373814].

46. Blanco-Aguirre ME, Kofman-Alfaro SH, Rivera-Vega MR, Medina C, Valdes-Flores M, Rizzo WB, Cuevas-Covarrubias SA. Unusual Clinical Presentation in Two Cases of Multiple Sulfatase Deficiency. Pediatr Dermatol 2001; 18:388-92. [PMID: 11737681].

47. Davis L, Abdi K, Machius M, Brautigam C, Tomchick DR, Bennett V, Michaely P. Localization and Structure of the Ankyrin-binding Site on ß2-Spectrin. J Biol Chem 2008; 284:6982-7. [PMID: 19098307].

48. Kim SY, Kim AR, Kim NK, Lee C, Kim MY, Jeon EH, Park WY, Choi BY. Unraveling of Enigmatic Hearing-Imparied GJB2 Single Heterozygotes by Massive Parallel Sequencing: DFNB1 or Not? Medicine (Baltimore) 2016; 95:e3029-[PMID: 27057829].

49. Meyer zum Gottesberge AM, Hansen S. The collagen receptor DDR1 co-localizes with the non-muscle myosin IIA in mice inner ear and contributes to the cytoarchitecture and stability of motile cells. Cell Tissue Res 2014; 358:729-36. [PMID: 25307162].

50. Chen W, Kahrizi K, Meyer NC, Riazalhosseini Y, Van Camp G, Najmabadi H, Smith RJ. Mutation of COL11A2 causes autosomal recessive non-syndromic hearing loss at the DFNB53 locus. J Med Genet 2005; 42:e61-[PMID: 16033917].

51. Shabbir MI, Ahmed ZM, Khan SY, Riazuddin S, Waryah AM, Khan SN, Camps RD, Ghosh M, Kabra M, Belyantseva IA, Friedman TB, Riazuddin S. Mutations of human TMHS cause recessively inherited non-syndromic hearing loss. J Med Genet 2006; 43:634-40. [PMID: 16459341].

52. Gao Z, Chi F, Huang Y, Yang J, Cong N, Li W. Expression of Numb and Numb-like in the development of mammalian auditory sensory epithelium. Neuroreport 2011; 22:49-54. [PMID: 21150807].

53. Ahram DF, Grozdanic SD, Kecova H, Henkes A, Collin RWJ, Kuehn MH. Variants in Nebulin (NEB) Are Linked to the Development of Familial Primary Angle Closure Glaucoma in Basset Hounds. PLoS One 2015; [PMID: 25938837].

54. Robertson NG, Morton CC. Beginning of a molecular era in hearing and deafness. Clin Genet 1999; 59:39-49. [PMID: 10334469].

55. Steel KP, Kros CJ. A genetic approach to understanding auditory function. Nat Genet 2001; 27:143-9. [PMID: 11175778].

56. Yu J, He S, Friedman JS, Akimoto M, Ghosh D, Mears AJ, Hicks D, Swaroop A. Altered Expression of Genes of the Bmp/Smad and Wnt/Calcium Signaling Pathways in the Cone-only Nrl-/- Mouse Retina, Revealed by Gene Profiling Using Custom cDNA Microarrays. J Biol Chem 2004; 279:42211-20. [PMID: 15292180].

Articles are provided courtesy of Emory University and the Zhongshan Ophthalmic Center, Sun Yat-sen University, P.R. China. The print version of this article was created on 3 February 2018. This reflects all typographical corrections and errata to the article through that date. Details of any changes may be found in the online version of the article.